Free Vibration and Dynamic Response Analysis by Petrov-Galerkin Natural Element Method

Jin-Rae Cho*, Hong-Woo Lee
School of Mechanical Engineering, Pusan National University,
Kumjung-Ku, Busan 609-735, Korea

In this paper, a Petrov-Galerkin natural element method (PG-NEM) based upon the natural neighbor concept is presented for the free vibration and dynamic response analyses of two-dimensional linear elastic structures. A problem domain is discretized with a finite number of nodes and the trial basis functions are defined with the help of the Voronoi diagram. Meanwhile, the test basis functions are supported by Delaunay triangles for the accurate and easy numerical integration with the conventional Gauss quadrature rule. The numerical accuracy and stability of the proposed method are verified through illustrative numerical tests.

1. Introduction

In order to minimize the inherent drawbacks of FEM, such as the element connectivity preservation, the numerical quality deterioration caused by the excessive mesh distortion and the troublesome mesh adaptation, the meshfree method was introduced by substituting finite elements with grid points (Nayroles, 1992). However, the grid-point-centered sub-domains in most meshfree methods (Belytschko et al., 1994 ; Liu et al., 1995 ; Duarte and Oden, 1996 ; Melenk and Babuska, 1996) are not perfectly separated but overlapped so that the grid-point-based basis functions in these methods do not obey the Kronecker delta property. Thus, the essential boundary treatment should require additional techniques (Belytschko et al., 1994 ; Zu and Atluri, 1998). Another critical issue of these methods is the need of background cell to utilize the conventional Gauss

quadrature rule for the numerical integration, owing to the irregular and overlapped supports of basis functions. What is worse, the numerical integration accuracy is remarkably influenced by how to construct the background cell.

Recently, the natural element method originated by Braun and Sambridge (1995) has been intensively explored as a possible solution to these drawbacks of meshfree methods (Sukumar et al., 1998). In which, the problem domain is discretized with a finite number of grid points, as in most meshfree methods. But, it uses Laplace interpolation functions (Belikov et al., 1997) defined with the help of Voronoi polygons and Delaunay triangles for both trial and test basis functions according to the natural neighbors and Bubnov-Galerkin approximation. These functions strictly satisfy the Kronecker delta property and this property allows the easy and accurate imposition of essential boundary condition. Furthermore, the natural element method does not require extra effort for constructing the background cell, because it utilizes a set of Delaunay triangles, which are identified automatically in the process of the basis function definition, as its background cell. Nevertheless, it suffers from the numerical integration difficulty as ever owing to the inconsist-

---

* Corresponding Author,
  E-mail : jrcho@pusan.ac.kr
  TEL : +82-51-510-2467; **FAX** : +82-51-514-7640
  School of Mechanical Engineering, Pusan National University, Kumjung-Ku, Busan 609-735, Korea. (Manuscript **Received** March 23, 2006; **Revised** August 4, 2006)

ency of the basis function supports with Delaunay triangles.

On the other hand, in the Petrov-Galerkin natural element method (Cho and Lee, 2006a) presented in this paper the test basis function is differently defined such that its support is identical with a union of Delaunay triangles, while Laplace interpolation function is taken for the trial basis function. Then, the above-mentioned inconsistency of Delaunay triangles with the supports of integrand functions contained in both stiffness matrix and load vector completely disappears. Thus, the application of the conventional Gauss quadrature rule to the background cell composed of Delaunay triangles can be accurately and simply performed.

This paper is an extension of our recent work (Cho and Lee, 2006a ; 2006b) to the free vibration and dynamic response analysis of 2-D linear elastic structures. The numerical accuracy and stability of the proposed method in the free vibration and dynamic response analysis are examined through illustrative numerical experiments. The structural dynamic problem is formulated with the Rayleigh-type damping model and time-integrated by the implicit Newmark scheme.

2. Natural Neighbor Interpolation

2.1 Voronoi polygons and delaunay triangles

For the sake of easy representation of the Voronoi diagram and the Delaunay triangulation, we consider a two-dimensional Euclidean space $\Re^2$. Referring to Fig. 1(a), we assume that a set $\aleph$ of distinct points called nodes : $\aleph = \{ x_1, x_2, \cdots, x_N \mid x_I \in \Re^2 \}$ is given in $\Re^2$, then the first-order Voronoi diagram V_I can be defined with N Voronoi polygons ω_N such that $V_I = \{ \omega_1, \omega_2, \cdots, \omega_N \mid \omega_1 \cup \cdots \cup \omega_N = \Re^2 \}$. By denoting $d(x, x_I)$ be the Euclidean metric in $\Re^2$, the Voronoi polygon ω_I corresponding to the I-th node is defined by

$$\omega_I = \{ x \in \Re^2 : d(x, x_I) < d(x, x_J), \forall J \neq I \} \quad (1)$$

The I-th Voronoi polygon ω_I is a sub-domain with its sides that perpendicularly bisect the lines connecting x_I and the adjacent neighbor nodes of I-th node x_I. A Voronoi polygon is uniquely defined to each node, and vertex points of each Voronoi polygon are called the Voronoi vertices. When node is located on the boundary of the convex hull $\Omega^{CH}(\aleph)$ of N points its Voronoi polygon becomes to be unbounded, referring to Fig. 1 (a), otherwise its Voronoi polygon is bounded. As shown in Fig. 1(b), the Delaunay triangulation as a geometric dual of the Voronoi diagram generates a set $\Im$ of Delaunay triangles $\triangle_{JKL}(x)$ such that

$$\Im \{ \triangle_{JKL}(x) ; \cup \overline{\triangle_{JKL}} = \Omega^{CH}(\aleph), J \neq K \neq L \} \quad (2)$$

where J, K and L refer to the nodes x_J, x_K and x_L in $\aleph$ which become three vertices of $\triangle_{JKL}$. In general, the convex hull becomes the problem

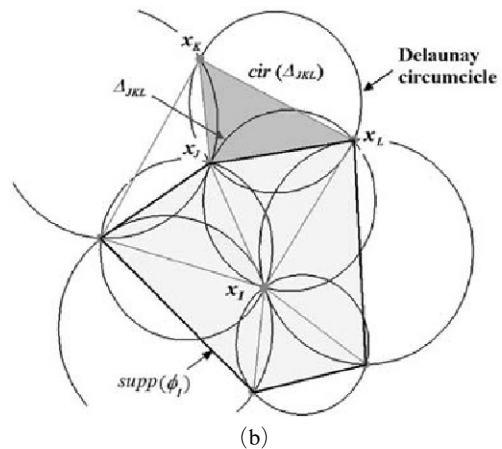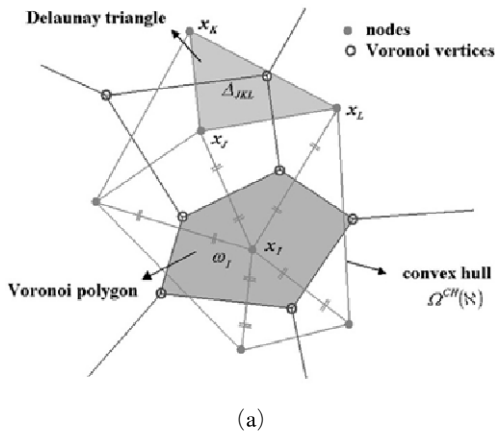

(a)   (b)

Fig. 1 Representation : (a) Voronoi diagram and Delaunay triangulation ; (b) Delaunay circumcircles

domain : $\Omega^{CH}(\aleph) \equiv \Omega$. Referring to Fig. 1(a), these three vertex nodes should be chosen such that three corresponding Voronoi polygons share common edges, and circumcircle defined by these three nodes is called the Delaunay circumcircle $cir(\Delta_{JKL})$. An important property of the Delaunay triangulation is the empty circumcircle criterion implying that individual Delaunay circumcircles should not contain any node in $\aleph$. Also, it is worth to note that the centers of these circumcircles are identical to the Voronoi vertices.

Referring to Fig. 1(a), the Voronoi polygon ω_I shares its sides with five Voronoi polygons, and such neighborhood polygons are called the natural neighbors of ω_I. In the same manner, the five nodes within five natural neighbors of ω_I are defined as the natural neighbors of the node x_I. These natural neighbors serve a basis for constructing Sibsonian and non-Sibsonian interpolation functions. The concept of the natural neighbors and the Sibsonian interpolation was introduced by Sibson (1980) originally for curve fitting and smoothing.

2.2 Laplace interpolation functions

Once the first-order Voronoi diagram and Delaunay triangulation were constructed, then Laplace interpolation functions corresponding to individual nodes x_I can be defined. Referring to Fig. 2(a), we describe how the I-th Laplace interpolation function ϕ_I is defined, where five cir-

cles are the Delaunay circumcircles generated by node x_I and its five neighbor nodes. We consider a point x_P within the region $\cup \overline{cir(\Delta_{IJK})}$ covered by these circumcircles, then we can does also define a new first-order Voronoi polygon ω_P which is composed of four sub-regions divided by the previously defined Voronoi polygons ω_I. These sub-regions are called the second-order Voronoi cells ω_{PI}, and those are geometrically defined by
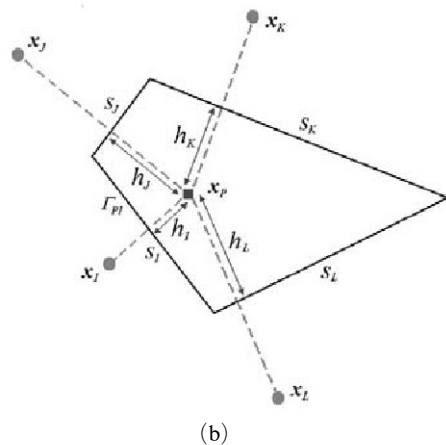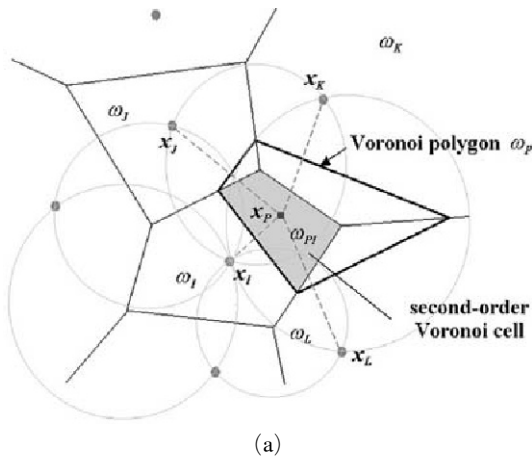
$$\omega_{PI} = \{ x \in \Re^2 : d(x, x_P) < d(x, x_I) < d(x, x_J), \\ \forall J \neq P, I \} \tag{3}$$

It is worthy noting that the shapes of Voronoi polygon ω_P and corresponding second-order Voronoi cells ω_{PI} vary with the location of point x_P.

In the Sibsonian interpolation method, interpolation functions are defined in terms of the relative area ratios of ω_{PI} to the total area of ω_P. On the other hand, Laplace interpolation functions in the non-Sibsonian case are expressed in the slightly different manner. Referring to Fig. 2 (b), we first introduce the weighting functions α_I defined by

$$\alpha_I(x_P) = \frac{s_I(x_P)}{h_I(x_P)}, \quad I = 1, 2, \cdots, M \tag{4}$$

where $s_I = |\gamma_{PI}|$, $h_I = d(x_P, x_I)/2$. Here, the subscript I designates the edge of ω_P facing to the node x_I and M denotes the number of natural neighbor nodes of the point x_P. Then, the value of Laplace interpolation function ϕ_I at point x_P is determined through

(a)   (b)

Fig. 2 Representation : (a) Second-order Voronoi cells ; (b) Geometric definition of the polygon ω_P

$$\phi_I(\boldsymbol{x}_P) = \alpha_I(\boldsymbol{x}_P) / \sum_{l=0}^{M} \alpha_l(\boldsymbol{x}_P) \qquad (5)$$

Since $\boldsymbol{x}_P$ is an arbitrary point within the support of ϕ_I we drop the subscript P hereafter. In this manner, all Laplace interpolation functions for a given node set $\aleph$ can be defined.

Laplace interpolation function ϕ_I is unity at its node $\boldsymbol{x}_I$ because h_I in Eq. (5) becomes infinity while the others of h_l remain finite. Referring to Cho and Lee (2006a), it vanishes along the whole boundary of its support, except for the Laplace interpolation functions corresponding to the nodes located on the boundary Γ of the convex hull $\Omega^{CH}(\aleph)$. Laplace interpolation function corresponding to the node located on the boundary Γ varies linearly from unity at its node to zero at its neighbor nodes along $supp(\phi_K) \backslash \Gamma$ but vanishes on the remaining part of its support boundary. $\Omega^{CH}(\aleph)$. Here, the support $supp(\phi_K)$ of ϕ_I becomes the intersection of the convex hull $\Omega^{CH}(\aleph)$ (i.e. the problem domain (Ω)) and the union $\cup \overline{cir(\Delta_{IJK})}$ of Delaunay circumcircles defined by the node $\boldsymbol{x}_I$ and its neighbor nodes (Farin, 1990) such that

$$supp(\phi_I(\boldsymbol{x})) = \cup \overline{cir(\Delta_{IJK}(\boldsymbol{x}))} \cap \Omega^{CH}(\aleph) \quad (6)$$

These behaviors of Laplace interpolation functions along the boundaries of their supports can be explained from the definition in Eq. (5). The reader may refer to Cho and Lee (2006a) for more detailed explanation.

3. 2-D Structural Dynamic Problem

3.1 Petrov-Galerkin natural element approximation

When restricted to a 2-D linear elastic body occupying the material domain $\Omega \in \Re^2$, its dynamic response $\boldsymbol{u}(\boldsymbol{x}; t)$ is governed by ($i,j = x,y$)

$$\sigma_{ij}(\boldsymbol{u})_{,j} - c\frac{\partial u_i}{\partial t} + b_i = \rho\frac{\partial^2 u_i}{\partial t^2} \text{ in } \Omega \times (0, T] \quad (7)$$

with initial and boundary conditions given by

$$u_i(0) = \dot{u}_i(0) = 0 \text{ in } \Omega \qquad (8)$$

$$u_i = \hat{u}_i \text{ on } \Gamma_D \times (0, T] \qquad (9)$$

$$\sigma_{ij} n_j = \hat{t}_i \text{ on } \Gamma_N \times (0, T] \qquad (10)$$

In which c, b_i and ρ indicate the damping coefficient, the body force components and the structure density, respectively. Meanwhile, Γ_D and Γ_N are the essential and natural boundary regions, T the time period of observation, and $\boldsymbol{n}$ the outward unit vector normal to the structure boundary $\Gamma = \overline{\Gamma_D \cup \Gamma_N}$. The virtual work principle converts the initial-boundary-value problem (7) into the variational formulation: Find $\boldsymbol{u}$ such that

$$\int_{\Omega} \left\{ \rho\frac{\partial^2 u_i}{\partial t^2} v_i + c\frac{\partial u_i}{\partial t} v_i + \sigma_{ij}(\boldsymbol{u})\varepsilon_{ij}(\boldsymbol{v}) \right\} d\Omega = \int_{\Omega} b_i v_i d\Omega + \int_{\Gamma_N} \hat{t}_i v_i ds \qquad (11)$$

for every admissible displacement $\boldsymbol{v}$.

In the Petrov-Galerkin natural element approximation, trial and test functions are expanded as follows:

$$u_i(\boldsymbol{x}; t) = \sum_{J=1}^{N} \bar{u}_i^J(t) \cdot \phi_J(\boldsymbol{x}) \qquad (12)$$

$$v_i(\boldsymbol{x}; t) = \sum_{I=1}^{N} \bar{v}_i^I(t) \cdot \Psi_I(\boldsymbol{x}) \qquad (13)$$

for a given natural element grid composed of N nodes. Here, ϕ_J are Laplace interpolation functions defined in the previous section, while ψ_I are the constant strain functions supported on Delaunay triangles that are defined by

$$\hat{\psi}_i(x, y) = \{(x_j y_k - x_k y_j) + (y_j - y_k)x + (x_k - x_j)y\}/2A, \ i,j,k = 1,2,3 \qquad (14)$$

Referring to Fig. 3, three points $\boldsymbol{x}_1, \boldsymbol{x}_2$ and $\boldsymbol{x}_3$ are
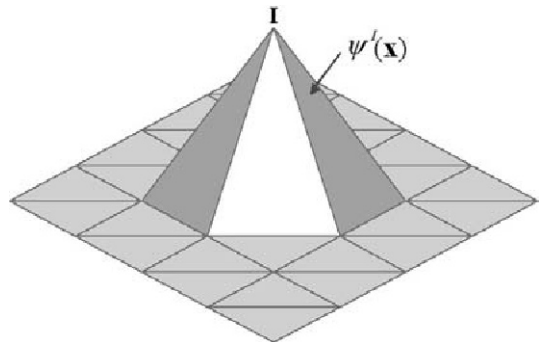

Fig. 3 Constant strain basis function supported on Delaunay triangle

three vertices of triangle (in the counter-clockwise direction) and A is the area of each triangle.

Introducing the $(2N \times 1)$ nodal vector $\bar{u}$ and substituting Eqs. (12) and (13) into Eq. (11) leads to the following semi-discrete matrix equations

$$\sum_I^N M^I \ddot{\bar{u}} + \sum_I^N C_I \dot{\bar{u}} + \sum_I^N K^I \bar{u} = \sum_I^N F^I \qquad (15)$$

The viscous damping is treated by the Rayleigh-type damping model : $C = \alpha M + \beta K$, and three node-wise matrices are defined by

$$M^I = \int_{\Omega_v^I} \rho \, \Psi^T \Phi d\Omega \qquad (16)$$

$$C^I = \int_{\Omega_v^I} c \, \Psi^T \Phi d\Omega \qquad (17)$$

$$K^I = \int_{\Omega_v^I} (D \Psi)^T E (D \Psi) d\Omega \qquad (18)$$

$$F^I = \int_{\Omega_v^I} \Psi^T b d\Omega + \int_{\Gamma_N \cap \Omega_v^I} \Psi^T \hat{t} ds \qquad (19)$$

with $\Omega_v^I = supp(\psi_I(x))$, the (3×3) matrix E of the two-dimensional linear elastic materials and the (3×2) divergence-like operator D defining Cauchy strains $\{\varepsilon_{xx}, \varepsilon_{yy}, 2\varepsilon_{xy}\}^T$. Other two matrices Ψ and Φ are in the form of

$$\Psi = \left[\begin{pmatrix} \psi_1 & 0 \\ 0 & \psi_1 \end{pmatrix} \cdots \begin{pmatrix} \psi_I & 0 \\ 0 & \psi_I \end{pmatrix} \cdots \begin{pmatrix} \psi_N & 0 \\ 0 & \psi_N \end{pmatrix} \right] \qquad (20)$$

$$\Phi = \left[\begin{pmatrix} \phi_1 & 0 \\ 0 & \phi_1 \end{pmatrix} \cdots \begin{pmatrix} \phi_J & 0 \\ 0 & \phi_J \end{pmatrix} \cdots \begin{pmatrix} \phi_N & 0 \\ 0 & \phi_N \end{pmatrix} \right] \qquad (21)$$

On the other hand, a simple harmonic motion of the solution vector $\bar{u}$ allows us to assume the explicit time function given by

$$\bar{u}(t) = \bar{u} e^{i\omega t} \qquad (22)$$

Substituting Eq. (22) into Eq. (15) without the load vector F_I ends up with the following eigen matrix system :

$$\left[\sum_I^N K^I - \omega^2 \sum_I^N M^I \right] \bar{u} = 0 \qquad (23)$$

3.2 Time-incremental numerical scheme

In order for the temporal discretization of the semi-discrete equations of motion (15), we divide the time period T of observation into a finite number of sub-intervals with the time step Δt. By replacing the node-wise matrices in Eq. (15) with the global matrices, together with the implicit time integration, we have

$$M \ddot{\bar{u}}^{t+\Delta t} + C \dot{\bar{u}}^{t+\Delta t} + C \bar{u}^{t+\Delta t} = F^{t+\Delta t} \qquad (24)$$

According to the Newmark's constant-averaged-acceleration method (Bathe, 1996), acceleration and velocity are discretized as

$$\ddot{\bar{u}}^{t+\Delta t} = \frac{2}{\gamma \Delta t} \left[\bar{u}^{t+\Delta t} - \bar{u}^t - \Delta t \dot{\bar{u}}^t - \frac{(1-\gamma)}{2} (\Delta t)^2 \ddot{\bar{u}}^t \right] \qquad (25)$$

$$\dot{\bar{u}}^{t+\Delta t} = \dot{\bar{u}}^t + (1-\delta) \Delta t \ddot{\bar{u}}^t + \delta \Delta t \ddot{\bar{u}}^{t+\Delta t} \qquad (26)$$

with $\gamma = \delta = 0.5$. Substituting Eqs. (25) and (26) into Eq. (24), one can determines the time-state-wise displacements using

$$\bar{u}^{t+\Delta t} = \tilde{K}^{-1} (F^{t+\Delta t} + M \bar{u}_m^t + C \bar{u}_c^t) \qquad (27)$$

where

$$\tilde{K} = K + \frac{2}{\gamma (\Delta t)^2} M + \frac{2\delta}{\gamma \Delta t} C \qquad (28)$$

$$\tilde{u}_m^t = \frac{2}{\gamma (\Delta t)^2} \bar{u}^t + \frac{2}{\gamma \Delta t} \dot{\bar{u}}^t + \frac{1-\gamma}{\gamma} \ddot{\bar{u}}^t \qquad (29)$$

$$\tilde{u}_c^t = \frac{2\delta}{\gamma \Delta t} \bar{u}^t + \frac{2\delta - \gamma}{\gamma} \dot{\bar{u}}^t + \frac{1-\gamma}{\Delta} t \ddot{\bar{u}}^t \qquad (30)$$

We next summarize the time-incremental solution algorithm for the damped dynamic response analysis by the Petrov-Galerkin natural element method.

Step 1. Grid generation
- Generate a set $\aleph$ of grid points x_P.
- Construct Voronoi polygons ω_I and Delaunay triangles $\Delta_{IJK}(x)$.
- Construct Delaunay circumcles $c_i r(\Delta_{IJK})$ and N Laplace interpolation functions.

Step 2. Initial calculation
- Form the stiffness matrix K and the mass matrix C.
- Calculate initial acceleration $\ddot{\bar{u}}^0$: $\ddot{\bar{u}}^0 = M^{-1} F^0$.
- Store initial values $\bar{u}^0, \dot{\bar{u}}^0$ and $\ddot{\bar{u}}^0$.
- Form the effective stiffness matrix $\tilde{K}$ from Eq. (28).

Step 3. At each time stage
- Form the effective nodal solution vectors $\tilde{u}_m^t$ and $\tilde{u}_c^t$.
- Solve Eq. (27) for displacements $\bar{u}^{t+\Delta t}$.

– Update acceleration $\ddot{\boldsymbol{u}}^{t+\Delta t}$ and velocity $\dot{\boldsymbol{u}}^{t+\Delta t}$ from Eqs. (25) and (26).

– Form the effective stiffness matrix $\widetilde{\boldsymbol{K}}$ and repeat Step 3.

4. Numerical Experiments

According to the theoretical results described so far, a PC-based test program was coded in Fortran in which the mass matrix is not lumped and its upper triangular part is stored. Numerical experiments are composed of the free vibration analysis and the dynamic response analysis without and with the viscous damping, and the numerical results are compared with those obtained by the Bubnov-Galerkin natural element method (BG-NEM) and the constant strain finite element method (CS-FEM).

4.1 Free vibration analysis

Fig. 4(a) shows an elastic tube with the inner radius $r=0.1$ m and the thickness $t=0.05$ m, for which the plane strain condition is assumed and

material properties are set by $\rho=7,800$ kg/m³, $E=210$ GPa and $\nu=0.3$. From the problem symmetry, a quarter of the tube is taken for the free vibration analysis with the uniform natural element grid composed 328 nodes, as shown in Fig. 4(b). But, the grid density is not fixed but changed for the next convergence assessment.

We employ Lanczos and Jacobi methods to compute lowest natural frequencies and modes $\{\omega_i, \bar{\boldsymbol{u}}_i\}$ up to the desired number. Four lowest mode shapes are represented in Fig. 5, where the second one is the extension mode. The extension modes display the low error level even if the approximation space is very poor (Petyt, 1990), so the convergence assessment focuses only on non-extension modes.

Next, we performed the convergence assessment of the PG-NEM in the free vibration analysis of the model problem. Figs. 6(a) and 6(b) compare the convergence rates of PG-NEM, BG-NEM and CS-FEM to the number of nodes for two lowest bending modes, where the relative frequency error η is defined by
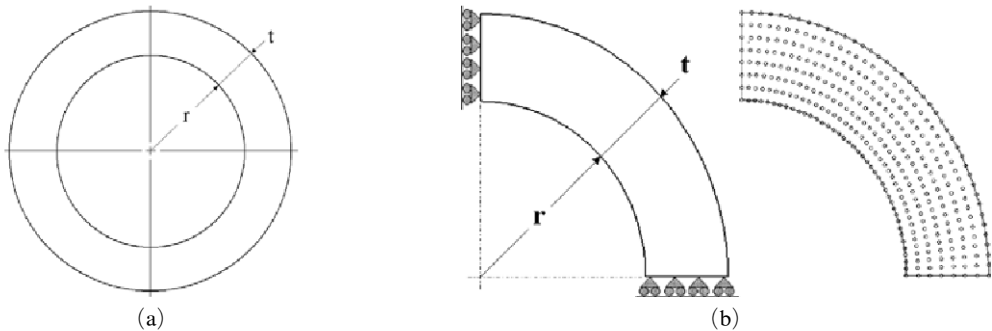

Fig. 4 An elastic tube : (a) Geometry ; (b) Natural element model and grid (328 nodes)
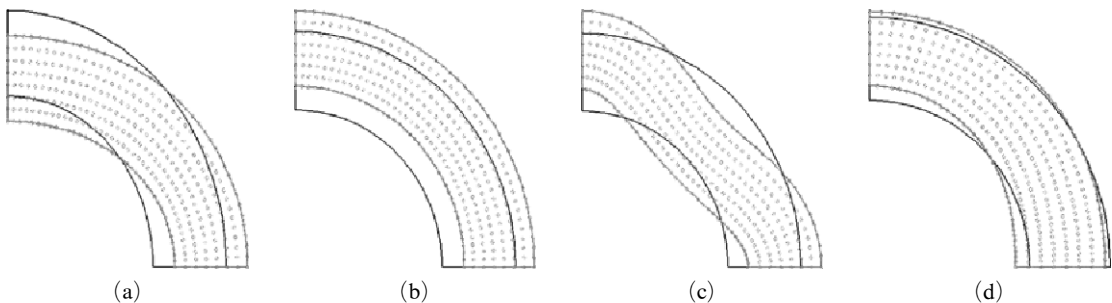

Fig. 5 Lowest four mode shapes : (a) First ; (b) Second ; (c) Third ; and (d) Fourth
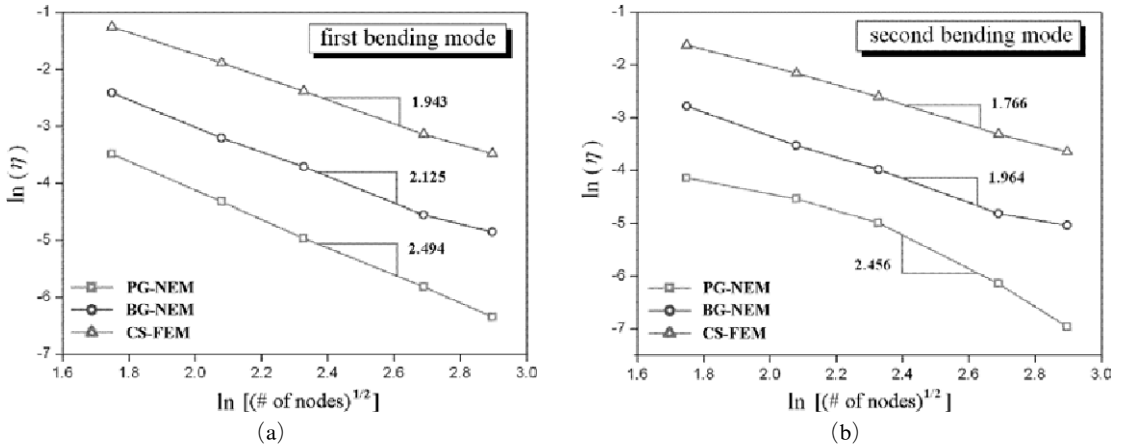
$$\eta = |\,\omega_{ref} - \omega^h\,|/|\,\omega_{ref}\,| \qquad (31)$$

Here, the reference frequency ω_{ref} was obtained by ANSYS commercial code using a fine mesh generated with uniform bi-linear elements (5,783 nodes). One can observe that PG-NEM shows higher convergence rates and lower absolute errors than other two methods for both bending modes. In particular, the convergence of BG-NEM is shown to be deteriorated at high grid density because the contribution of the numerical integration inaccuracy to the total numerical error becomes prominent.
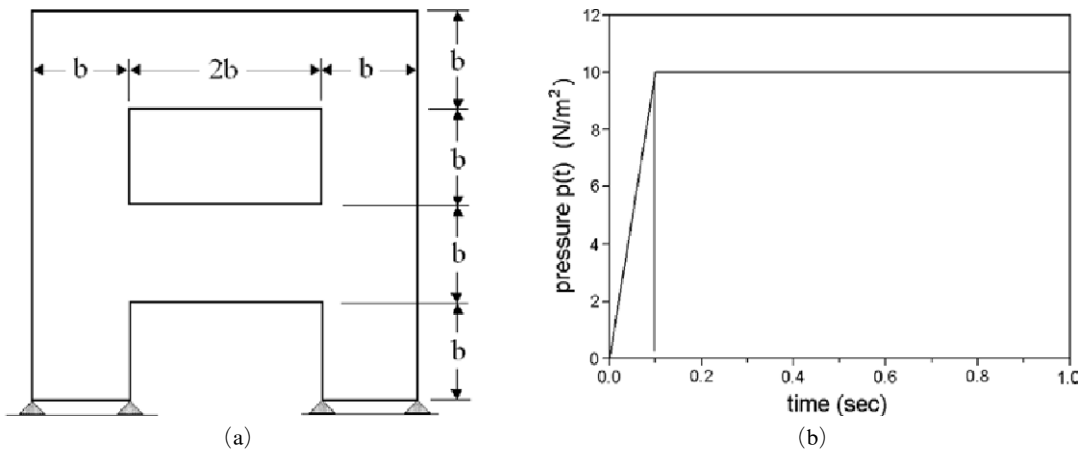
4.2 Dynamic response analysis

In order to assess the numerical accuracy and stability of the Petrov–Galerkin natural element method in the dynamic response analysis, we consider a two-dimensional frame structure depicted in Fig. 7(a). The frame is assumed in the plane sress condition and geometry and material parameters are taken as follows : $b=0.25$ m, $E=3.0$ MPa, $\nu=0.25$ and $\rho=3,000$ kg/m³. A pressure load $p(t)$ with the ramp time dependence represented in Fig. 7(b) is applied to the top surface of the frame. The dynamic response is investigated into the undamped and the damped cases, and the time integration up to 1.0 second by the Newmark scheme given in Eqs. (24)–(26) is performed with the uniform time step Δt of 0.005 sec.

Fig. 6 Convergence rates of natural frequencies : (a) First bending mode ; (b) Second bending mode

Fig. 7 Frame structure subject to dynamic pressure at the top surface : (a) Geometry ; (b) Time variation of the pressure

The problem symmetry allows us to model a half of the frame for the numerical experiment, as shown in Fig. 8, and two uniform grids (coarse and fine grids) are used for the accuracy study.

The numerical results of PG-NEM are compared with those obtained by BG-NEM and CS-FEM with the same grid densities set for PG-NEM. The reference solutions are obtained by MSC/MARC
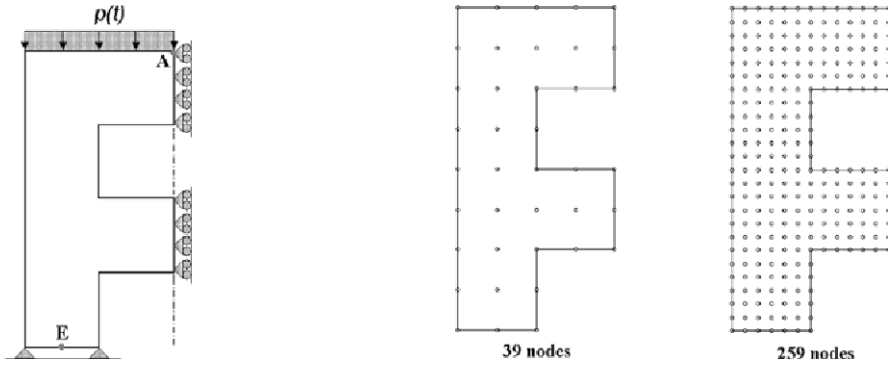

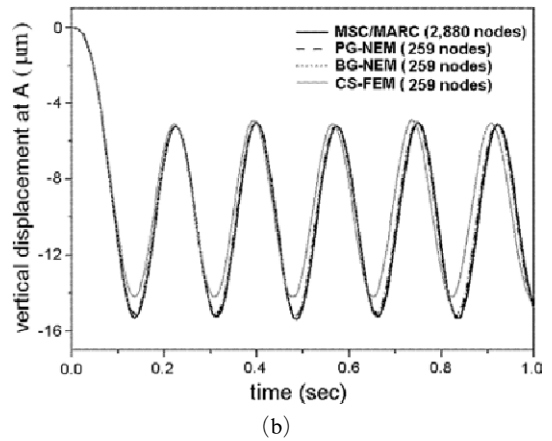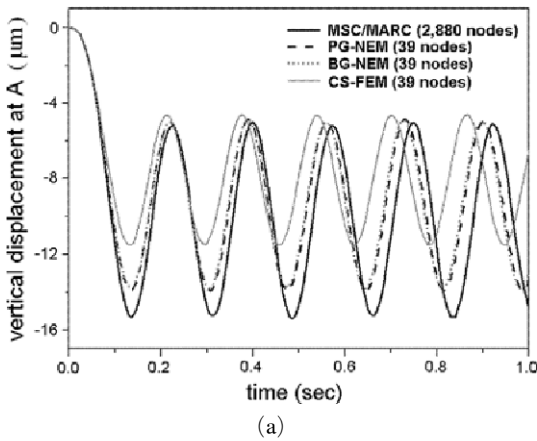**Fig. 8**   Natural element model and two uniform grids

(a)

(b)

Fig. 9   Time history of the vertical displacement at A (undamped) : (a) 39 nodes ; (b) 259 nodes
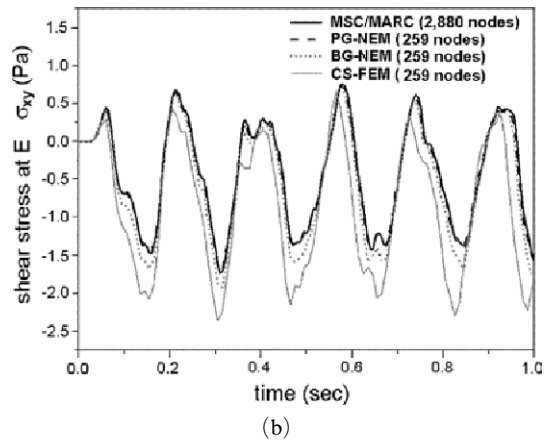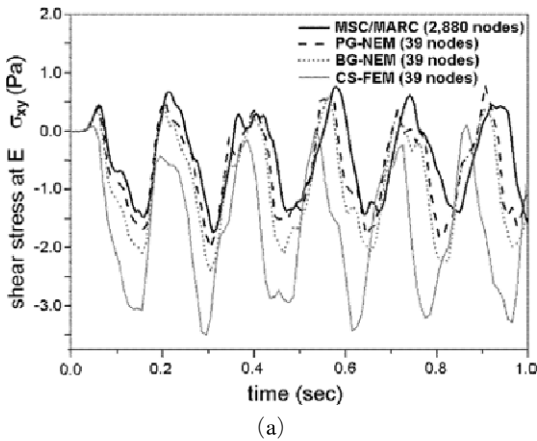

(a)

(b)

Fig. 10   Time history of the shear stress at E (undamped) : (a) 39 nodes ; (b) 259 nodes
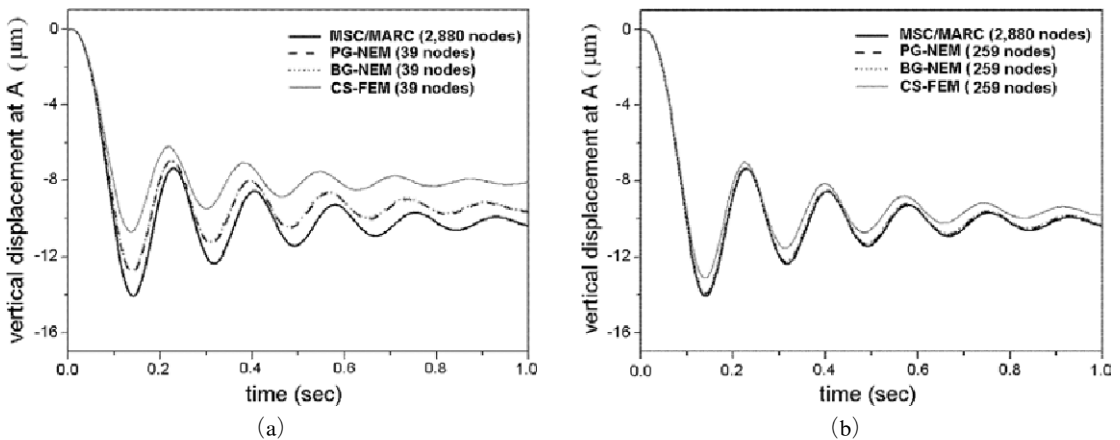
commercial code using a fine mesh generated with uniform bi-linear elements (2,880 nodes). In the current study, time histories of the displacement and the shear stress are investigated to the grid density and the approximation method.
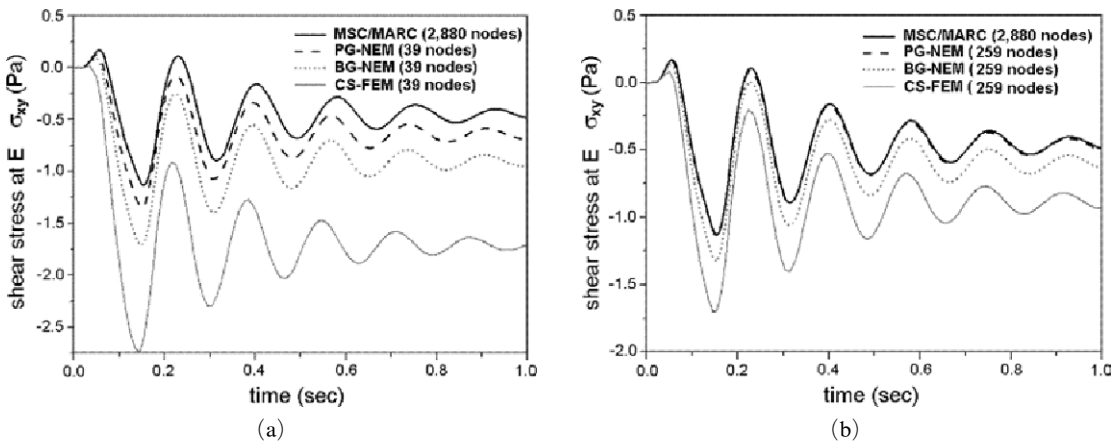
Figures 9 and 10 represent the time histories of the vertical displacement at A and the shear stress σ_{xy} at E of the undamped frame structure, respectively. The vertical displacements obtained by PG- and BG-NEM approach the reference solution as the grid density increases, whereas one by CS-FEM shows the remarkable difference even for fine mesh. This clearly shows that Laplace interpolation functions provide higher interpolation accuracy than finite element basis functions for the given same total number of nodes. The re-

lative accuracy of PG- and BG-NEM with respect to CS-FEM is also confirmed from Fig. 10, where PG-NEM with 259 nodes shows an excellent agreement with the reference solution. But, one can observe that BG-NEM provides lower accuracy than PG-NEM for both coarse and fine grids, and which is because the numerical integration inaccuracy of BG-NEM gives rise to the significant effect to the stress level. In general, the inconsistency of the basis function support and the background cell leads to the numerical accuracy deterioration and the non-uniformity in the stress field (Cho and Lee, 2006a).

The dynamic responses of the damped frame structure are represented in Figs. 11 and 12, for which two damping parameters α and β are set

(a)   (b)

Fig. 11   Time history of the vertical displacement at A (damped) : (a) 39 nodes ; (b) 259 nodes

(a)   (b)

Fig. 12   Time history of the shear stress at E (damped) : (a) 39 nodes ; (b) 259 nodes

by 0.005. Due to the damping effect, both the vertical displacement at A and the shear stress at E decay with the lapse of time. As in the undamped case, both PG- and BG-NEM shows higher numerical accuracy than CS-FEM, and PG-NEM provides the best accuracy. And, BG-NEM suffers from the numerical accuracy deterioration in the time-history prediction of shear stress owing to the numerical integration inaccuracy.

5. Conclusions

A Petrov-Galerkin natural element method (PG-NEM) has been introduced for the accurate free vibration and dynamic response analysis of two-dimensional linear elastic bodies. The combined use of Laplace interpolation functions (for the trial basis function) defined in terms of Voronoi polygons and the constant-strain test basis functions supported on Delaunay triangles completely eliminates the numerical integration error encountered in most meshfree methods, while preserving the higher interpolation accuracy of the Bubnov-Galerkin natural element method (BG-NEM).

These advantages of the proposed method have been verified through the illustrative numerical experiments. The benchmark free vibration test confirmed that PG-NEM provides the highest convergence rate with the lowest absolute error. And, the undamped and damped dynamic responses obtained by PG-NEM shows an excellent agreement with the reference solution, while CS-FEM produces the significant error and BG-NEM leads to the remarkable discrepancy owing to the numerical integration inaccuracy.

References

Bathe, K. J., 1996, *Finite Element Procedures*, Prentice-Hall, Singapore.

Belikov, V. V., Ivanov, V. D., Kontorovich, K. K., Korytnik, S. A. and Semenov, A. Su, 1997, "The Non-Sibsonian Interpolation : a New Method of Interpolation of the Values of a Function on an Arbitrary Set of Points," *Computational Mathematics and Mathematical Physics*, Vol. 37, pp. 9~15.

Belytschko, T., Lu, Y. Y. and Gu, L., 1994, "Element-free Galerkin Methods," *Int. J. Numer. Methods Engng.*, Vol. 37, pp. 229~256.

Braun, J. and Sambridge, M., 1995, "A Numerical Method for Solving Differential Equations on Highly Irregular Evolving Grids," *Nature*, Vol. 376, pp. 655~660.

Cho, J. R. and Lee, H. W., 2006, "A Petrov-Galerkin Natural Element Method Securing the Numerical Integration Accuracy," *J. Mech. Sci. Technol.*, Vol. 20, No. 1, pp. 94~109.

Cho, J. R. and Lee, H. W., 2006, "2-D Large Deformation Analysis of Nearly Incompressible Body by Natural Element Method," *Computers & Structures*, Vol. 84, pp. 293~304.

Duarte, C. A. and Oden, J. T., 1996, "An h-p Adaptive Method using Clouds," Comput. *Methods in Appl. Mech. Engrg.*, Vol. 139, pp. 237~262.

Farin, G., 1990, "Surface over Dirichlet Tessellations," *Computer Aided Geometric Design*, Vol. 7, No. 1-4, pp. 281~292.

Liu, W. K., Jun, S. and Zhang, Y. F., 1995, "Reproducing Kernel Particle Methods," *Int. J. Numer. Methods Fluids*, Vol. 20, pp. 1081~1106.

Melenk, J. M. and Babuska, I., 1996, "The Partition of Unity Finite Element Method : Basic Theory and Applications," *Comput. Methods Appl. Mech. Engrg.*, Vol. 139, pp. 289~314.

Nayroles, B., 1992, "Generalizing the Finite Element Method : Diffuse Approximation and Diffuse Elements," *Computational Mechanics*, Vol. 10, pp. 307~318.

Petyt, M., 1990, *Introduction to Finite Element Vibration Analysis*, Cambridge University Press, New York.

Sibson, R., 1980, "A Vector Identity for Dirichlet Tessellation," *Mathematical Proceedings of Cambridge Philosophical Society*, Vol. 80, pp. 151~155.

Sukumar, N., Moran, A. and Belytschko, T., 1998, "The Natural Element Method in Solid Mechanics," *Int. J. Numer. Methods Engng.*, Vol. 43, pp. 839~887.

Zu, T. and Atluri, S. N., 1998, "A Modified Collocation Method and a Penalty Formulation for Enforcing the Essential Boundary Condition in the Element Galerkin Method," *Computational Mechanics*, Vo. 21, pp. 211~222.